Resilient wide-area multi-mode controller design based on Bat algorithm for power systems with renewable power generation and battery energy storage systems

by Awan Uji Krismanto

Submission date: 24-Feb-2021 11:25AM (UTC+0700)
Submission ID: 1516760103
File name: Resilient_wide-area_multi-mode_controller.pdf (2.9M)
Word count: 7390
Character count: 37975

IET Generation, Transmission & Distribution

Research Article

IET Journals
The Institution of Engineering and Technology

Resilient wide-area multi-mode controller design based on Bat algorithm for power systems with renewable power generation and battery energy storage systems

ISSN 1751-8687
Received on 15th August 2018
Revised 14th January 2019
Accepted on 21st February 2019
doi: 10.1049/iet-gtd.2018.6384
www.ietdl.org

Herlambang Setiadi[1], N. Mithulananthan[1] ✉, Rakibuzzaman Shah[2,3], Kwang Y. Lee[4], Awan Uji Krismanto[1]

[1]*School of Information Technology & Electrical Engineering, The University of Queensland, QLD 4072, Australia*
[2]*School of Electrical and Electronic Engineering, The University of Manchester, M13 9PL, UK*
[3]*School of Engineering and Technology, CQ University, WA 6000, Australia*
[4]*Department of Electrical & Computer Engineering, Baylor University, Texas 76798, USA*
✉ *E-mail: mithulan@itee.uq.edu.au*

Abstract: Modern power systems consist of power electronics devices, which are used in energy conversion, especially in renewable energy sources as well as in load side to make the electricity consumption more efficient. However, these devices and their controllers could bring new challenges to power system stability, especially oscillatory stability. Apart from this, another challenge associated with renewable energy generation is the uncertainty in their power output. Hence, the integration of battery energy storage systems (BESSs) is being developed to minimise the uncertainty and variability in renewables. Furthermore, to tackle the complex dynamics and inertia-less characteristics of wind and solar power plants additional controllers such as power oscillation damping (POD) control and virtual inertia scheme are sought. Moreover, as the oscillation could originate from different locations and affect several areas in power system, utilising wide-area signals for damping control is essential. However, the primary challenges associated with the wide-area oscillation damping controller are signal transmission delay, loss of communication signal, data drops, and others. A controller that is resilient to all or most of the potential drawbacks is required. Hence, this paper proposes a resilient wide-area multi-mode controller (MMC) for solving oscillatory stability problems with high penetration of renewable power generations (RPGs) and BESSs. To get the optimal design with uncertainties, a contemporary heuristic optimisation technique called bat algorithm (BA) is used here. The practical power system of Java 500 kV Indonesian grid is used to evaluate the performance of the resilient wide-area MMC. From the results, it is found that the proposed controller effectively damp the critical mode of oscillation in the system. It is also observed that the proposed controller can tackle the problems of communication failure as well as certain damping controller failures.

Q1

1 Introduction

Oscillatory stability or small-signal stability is the subclass of rotor angle stability and often referred as small-signal angle stability. This instability problem could emerge due to the lack of the damping torque in a single or group of synchronous machines. Traditionally, this instability could emerge due to load changes, weak interlink, and inappropriately designed controller. Modern power system will consist of huge amount of renewable power generation (RPG) such as wind power plants (WPPs) and large-scale photovoltaic (PV) plants. In order to facilitate remote large-scale RPG, a large number of high-voltage direct current (HVDC) links are also expected in future grids along with electric vehicle (EV) charging stations. The integration of these new and emerging technologies could affect the rotor angle and frequency stability of the system due to distinct inertia-less characteristics and uncertainty in the power output [1–4].

As reported in [5], the integration of EV charging stations may affect the oscillatory stability margin of the system. The impact of HVDC on small-signal stability is reported in [6]. The influence of large-scale PV plants on the small-signal stability is reported in [7]. As reported in [7], the integration of large-scale PV plant may adversely affect the oscillatory stability of power system due to zero inertia and reverse power flow. The influence of WPP penetration on small-signal stability is reported in [8]. Furthermore, the impact of power output uncertainty of both WPP and PV plants are reported in [9, 10]. It has been revealed that uncertainty associated with WPP and PV could affect the oscillatory stability of the system. To handle the uncertainty in power output of the RPG, additional devices such as battery energy storage systems (BESSs) can be utilised.

As reported in [11], the integration of BESS could enhance the voltage stability of power systems. It could also be used for frequency stability enhancement as described in [12]. Furthermore, the integration of BESS may positively affect the oscillatory stability of power systems as stated in [13]. The variability in power generation may be compensated by integrating BESS into power systems. However, without any additional controller, BESS may minimally affect the small-signal and frequency stability of the system. The power oscillation damping (POD) controller can be used in the BESS for low-frequency oscillation damping.

The application of POD with wide area signals is reported in [14, 15]. In [14], a wide-area POD is installed in the HVDC system as an additional controller for damping the oscillation of the host AC system. In [15], the wide-area POD is installed in the excitation systems of the generator to enhance the small-signal stability performance of power systems. In both cases ([14] and [15]), numerical studies are performed in the real-time digital simulator (RTDS).

One of the challenges of wide-area POD integration is the latency of control input signals. This problems may become worst if the signal is coming from distant sources. The impact of time delay or signal latency of the POD is testified in [16]. A fast and reliable communication system is required for the effective wide-area POD. Although the existing methods ensure the reliability of communication to a certain degree, still there is a possibility of communication failures or disruptions. Hence, designing a controller that is resilient to communication failure is essential. Wide-area POD resilient to the communication failure is reported in [17]. In [17], the resilient wide-area POD is used as additional controller in voltage source converter HVDC. However, the implication of control signal loss to actuator or controller failure

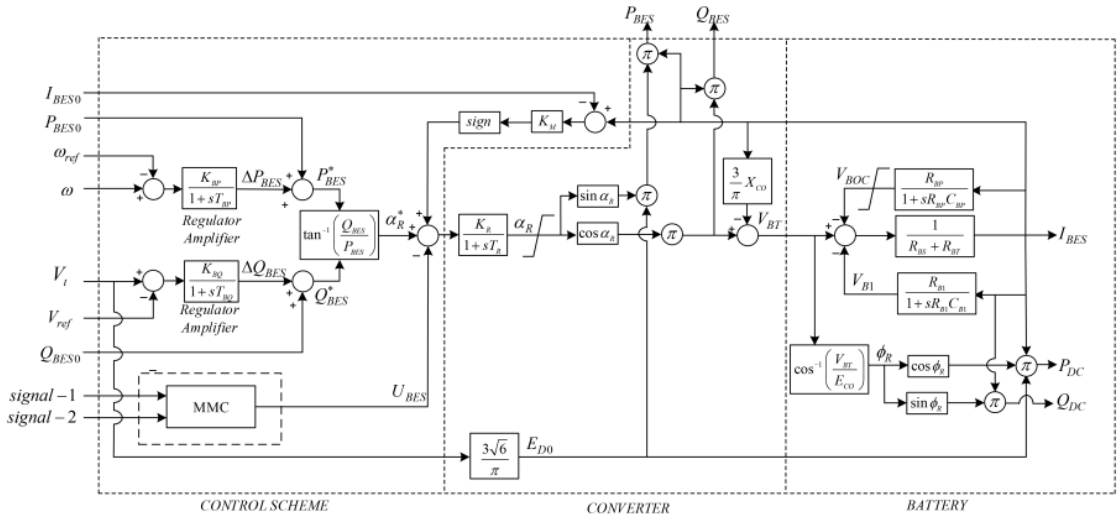

Fig. 1 *Dynamic model of BESS*

was not considered in [17] and other references given therein. Hence, it is essential to design the controller that is resilient not only to signal losses but also to controller failures.

Another problem for such resilient control design is the mathematical burden due to various distinct characteristics of different devices and controls in future power system. Hence, designing the controller using traditional mathematical approach is not obliging. Hence, the controller design based on the meta-heuristic algorithm can be utilised to minimise the complexity of designing the controller, at the same time achieving the best performance.

The application of meta-heuristic algorithms for solving complex power system problems are developed very fast over the past decades [18]. The use of differential evolution algorithm for designing power system stabiliser and static synchronous compensator is reported in [19]. The utilisation of particle swarm optimisation (PSO) for stochastic optimal operation of microgrid is stated in [20]. In addition, other swarm optimisation techniques, such as ant colony system and artificial bee colony, are applied to solve economic emission dispatch and optimal load flow problems [21, 22]. Among all proposed methods, the bat algorithm (BA) is appearing more popular due to simple algorithm and fast computational process. Hence, this paper aims to design a wide-area resilient controller using BA algorithm. The main contributions of this paper can be stated as follows:

1. Design a wide-area resilient MMC considering the integration of RPG and BESS with the communication or any other controller failure.
2. Utilisation of the BA algorithm to design a wide-area resilient MMC to overcome the mathematical burden for designing the POD controller.
3. Evaluation of the effectiveness of the proposed control in a representative dynamic model of a realistic power system.
4. Comprehensive ranking of controller performance based on the new approach.

The rest of the paper is organised as follows: Section 2 provides the overview of BESS and RPG models. A number of indices for control performance assessment are described in Section 3. Section 4 briefly explains the mathematical model of MMC structure, BA algorithm, the control objectives, and the controller design procedure. Results and discussions are presented in Section 5. Finally, Section 6 highlights the main contributions and conclusions of this work.

2 Modelling overview

2.1 Battery energy storage system model

Apprehending the dynamic behaviour of BESS including associated controller is essential for oscillatory stability studies. The dynamic behaviour of BESS for oscillatory stability can be captured by the model proposed in [23]. This model consists of three-phase transformer, converter, battery cells, and controllers. In this study, the transformer is modelled as ideal transformer, while the battery cell has been modelled as a second-order model. Furthermore, the converter and the associated controller is modelled as a first-order model. Fig. 1 shows the dynamic model of BESS used in this study. The parameters used in this work are taken from [23].

2.2 Renewable power generation model

Large-scale PV and WPP are considered as RPG for this study. The dynamic model of a large-scale PV developed by North American Electric Reliability Corporation (NERC) and Western Electricity Coordination Council (WECC) is used here [24, 25]. The dynamic model consists of the converter and associated controller dynamics. The first-order converter model presents the inverter dynamics of the PV plant. The converter controller comprises of converter current limiter and the PI controller for reactive power control. The dynamics of the maximum power point tracking (MPPT) is ignored as the PV system is considered to be operating at the maximum power point [26]. Here, the WPP model consists of dynamic representation of wind turbine, permanent magnet synchronous generator, rotor, and grid-side converter with the associated controllers. The complete dynamic model of the WPP used here can be found in [27] and the references therein.

3 Controller performance ranking

Three different controller performance ranking methods are used here. The first ranking index is the performance ranking. The performance ranking index investigates both the eigenvalue analysis and time domain simulation to evaluate the controller performance. The mathematical representation of controller performance ranking method can be described as [28]:

$$R^{Per} = w^{\xi}N[\xi^{\text{Contr}} - \xi^{\text{Base}}] + w^{\tau}N[\tau^{\text{Contr}} - \tau^{\text{Base}}] + w^{\Delta\omega}N[\Delta\omega^{\text{Contr}} - \Delta\omega^{\text{Base}}] \quad (1)$$

In (1), w^{ξ}, w^{τ} and $w^{\Delta\omega}$ are weighting factors for the damping, settling time, and overshoot of the rotor speed. The value of weighting factors are, respectively, 0.4, 0.4, and 0.2. The N indicates the normalisation of these factors with value ranging from

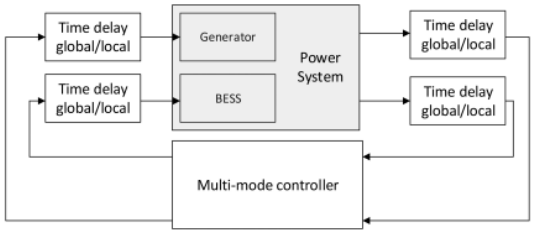

Fig. 2 *Overall power system structure*

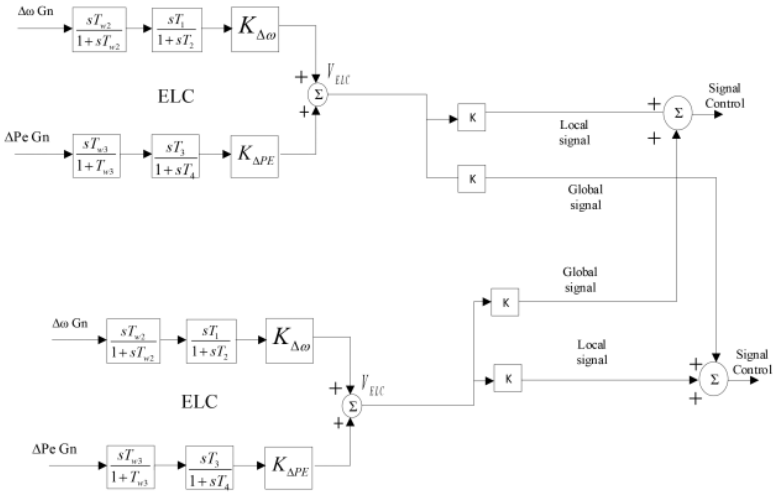

Fig. 3 *Multi-mode controller (MMC) structure*

0 to 1 based on all observed values for the different controller tested. The normalisation factors are used to make all of the observed values ranging from 0 to 1. The *Contr* and *Base* superscripts indicate the system with controller and base condition (BC), respectively.

The second controller performance ranking method is used to assess the robustness. In this ranking method, the controller performance is assessed by determining how the system performed with different system conditions. The generation output and loading conditions are included for assessing this index. This ranking method can be calculated as [28]:

$$R^{\text{rob}} = w^{\text{all}} N\left[\frac{1}{M}\sum_{1}^{M}\left(\xi^{\text{Contr}} - \xi^{\text{Base}}\right)\right] + w^{\text{min}} N\left[\xi_{\text{min}}^{\text{Contr}} - \xi_{\text{min}}^{\text{Base}}\right] \quad (2)$$

In (2), w^{all} and w^{min} are the weighting factor for all condition and the minimum damping comparison with 0.5 as the value of each weighting factor. While M indicates the number of operating conditions and the subscript min related to the operating condition where the minimum damping enhancement is achieved. The last performance ranking method is the simplicity ranking. The mathematical representation of this rank can be described as [28]:

$$R^{\text{sim}} = w^{t} N[(t^{\text{Contr}})^{-1}] + w^{c} N[(t^{\text{Code}})^{-1}] + w^{p} N[p^{\text{Contr}}] \quad (3)$$

In (3). t^{Contr}, t^{Code}, and p^{Contr} are controller tuning time, number of code line, and personal score related to the simplicity. The weighting factors of tuning time, number of code lines, and personal score are indicated by w^{t}, w^{t} and w^{t} with value 0.6, 0.3, and 0.1 [28]. The other controller performance indices used here are given in the Appendix.

4 Controller design

4.1 Wide-area resilient multi-mode controller

The concept of the multi-mode controller (MMC) is to design multiple controllers to enhance the damping of a particular critical mode or weak modes. In this particular design method, if one controller is not operating correctly, then other controllers can work as a backup. The controller is resilient to the communication failure due to the multi-input multi-output structure. Fig. 2 illustrates the structure of the overall power system including BESS and multi-mode POD controller, while Fig. 3 shows the detailed MMC structure.

As shown in Fig. 3, the given controller consists of an external linear controller (ELC) and gain constants. The ELC is installed in each generator, while the input of the MMC is a combination of the ELC outputs in each generator scaled by the gain constants. Furthermore, the output of the resilient controller is a control signal to the excitation system and BESS outer controller.

Here, the time delay of global signal for BESS and generator excitation controller has the same value (i.e. 700 ms). In contrast, the time delay with any local signal to BESS and generator excitation system is different. The time delay of the local signal for generator excitation is 10 ms, while the BESS local signal time delay is 100 ms. The local signal to BESS is from the generator in a different location within the same area; therefore, higher time delay (i.e. 100 ms) has been considered. The time delay associated with control input from the controller to the excitation system is 10 ms, while the delay associated with control input from the controller to the BESS is modelled as 100 ms. The time delay model used here is given in the Appendix.

4.2 Bat algorithm

BA was first introduced by Xin She Yang in 2010 [29]. This algorithm is inspired by the behaviour of bats to find food. To find nest, detecting food, and avoid obstacles in the dark, Bat used some

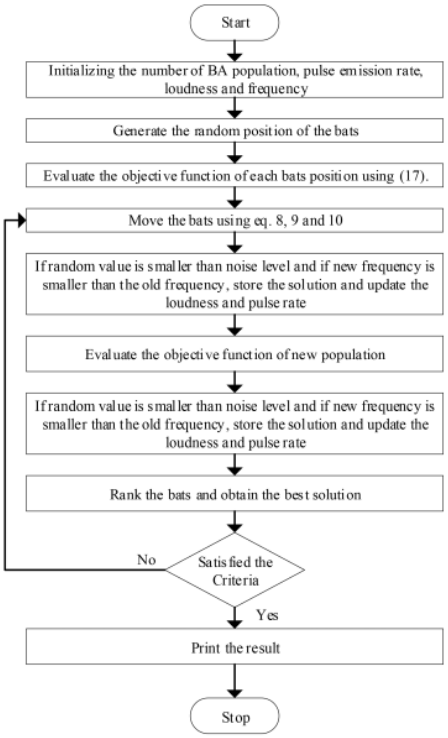

Fig. 4 *BA flowchart*

kind of sonar signals called an echolocation. Bats are able to fly in the night (as bats are considered as nocturnal animals) without crashing with objects by using the echolocation abilities. By considering the characteristic of bats, the BA can be designed by using the following [29]:

- The distance, food, and obstacles are determined by using the echolocation behaviour.
- Speed, position, frequency, and loudness are described as v_i, x_i, f_i, and A_i. It should be noted that bats randomly fly to find food. Here, frequency represents modulated signals from the sonar signals of bats. While loudness represents the volume of the sonar signals. This volume of the signals is varied from loudest when searching for prey to quitter when homing towards the prey.
- The loudness level varies from maximum (A_0) to minimum value ($A_{\min}$) and the dimension to find the space are indicated by d_i

Here, x_it and v_i^t present the new position and velocity of the bats. Furthermore, the mathematical representation of bat velocity and position can be calculated using (5) and (6) [29]:

$$f_i = f_{\min} + (f_{\max} - f_{\min})\beta \tag{4}$$

$$v_i^{t+1} = v_i^t + (x_i^t - x^*)f_i \tag{5}$$

$$x_i^{t+1} = x_i^t + v_i^t \tag{6}$$

In (5), x^* represents the optimal location after comparing all the solutions among all bats in each iteration. Furthermore, β is a random vector taken from the uniform distribution. Moreover, by multiplying f_i the velocity of the bats is increased. Furthermore, $f_{\min}$ and $f_{\max}$ are applied depending the requirement of the systems (usually the value of $f_{\min}$ is 0 and $f_{\max}$ is 100). Initially, each bat is randomly assigned a frequency which is drawn uniformly from [$f_{\min}$, $f_{\max}$] [29].

In each iterations process, the pulse emission (r_i) and loudness (A_i) from bats are updated. When bats find the prey, the noise levels of bats are decreased, while the pulse of the bats are increased. The value of maximum and minimum noise can be selected according to the requirement. For the simplicity, the maximum and minimum value of noise can be set to 1 and 0 by assuming that when noise level is 0, the bats found their prey and temporarily stopped emitting sound. Those activity can be mathematically expressed by (7) and (8) [29]:

$$A_i^{t+1} = \alpha A_i^t \tag{7}$$

$$r_i^{t+1} = r_i^0[1 - \exp(-\gamma t)] \tag{8}$$

In (7) and (8), r_i is the pulse emission, and α and γ are constants value of alpha and gamma. For every $0 < \alpha < 1$ and $\gamma > 0$, the mathematical representation of the noise level can be described by (9). For simplicity, the value of α and γ can be set with the same value between 0–1 [29]. Here, the parameters of MMC are determined as the bat's position. Fig. 4 illustrates the flow diagram of the BA.

$$A_i^t \to 0, r_i^t \to r_i^0, t \to \sim \tag{9}$$

4.3 Objective function

Here, a multi-objective function is used. The first objective function is to move the real parts of the eigenvalue to the left half plane. It can be described as

$$J_1 = \sum_{\sigma_0 \geq \sigma_i} [\sigma_0 - \sigma_i]^2 \tag{10}$$

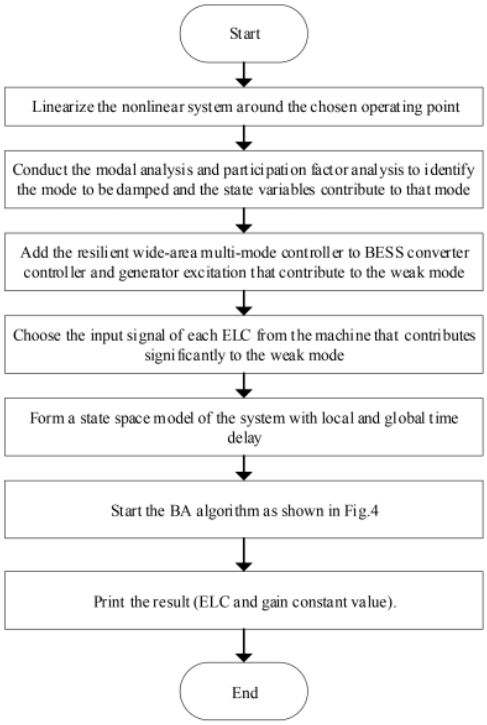

Fig. 5 *Flow diagram for controller design*

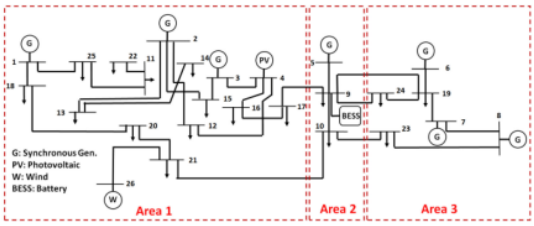

Fig. 6 *Java 500 kV Indonesian grid with RPG and BESS*

Table 1 EM mode of Java grid

Mode	Damping	Participation of the generator
inter-area	2.07	*G*3, *G*5
local 1	9.07	*G*6
local 2	2.11	*G*5
local 3	6.26	*G*1
local 4	6.25	*G*2
local 5	26.84	*G*7, *G*8
local 6	18.09	*G*8, *G*7

In (10), σ_i and σ_0 are the real parts of the ith mode and the desired mode location, respectively. The second objective function makes sure that the critical mode has the damping ratio >5%. The mathematical representation of the second objective function can be described as

$$J_2 = \sum_{\xi_0 \le \xi_i} [\xi_0 - \xi_i]^2 \tag{11}$$

In (11), ξ_i and ξ_0 are the damping ratio of the ith eigenvalue and the desired damping value, respectively. The third objective function is used to make sure that the non-linear response of the system has the minimum error compared to the steady-state value. This objective function measures how high is the overshoot and how fast the settling time of the system. The mathematical representation of the third objective function can be calculated using as in (12):

$$J_3 = \sum \int_0^{t_1} t\,|\Delta\omega(t, X)|\,dt \tag{12}$$

In (12), $\Delta\omega(t, X)$ is the oscillatory condition of generator rotor speed that contributed into the weak modes, X consists of MMC parameters, while t_1 is the time frame of the simulation. The rotor speed signals are used in the objective function. The representation of the objective function here can be expressed as in (13).

$$\text{Objective} = \min\,(aJ_1 + bJ_2 + cJ_3) \tag{13}$$

Subject to:

$$\begin{aligned} 10 \le T_{W2}, T_{W3} \le 20 \\ 0.05 \le T_1 \le 0.1 \\ 0.02 \le T_2 \le 0.1 \\ 0.03 \le T_3 \le 0.1 \\ 0.01 \le T_4 \le 0.1 \\ 5 \le K_{\Delta\omega n} \le 20 \\ 1 \le K_{\Delta pen} \le 2 \\ 50 \le K_n \le 100 \end{aligned} \tag{14}$$

In (13), a, b, and c are the weighting factors in the range of 1–0. Fig. 5 illustrates the flow diagram for the resilient wide-area MMC design using BA.

In addition to the objective function, upper and lower limit bounds given in (13) and (14) are used to get better damping performance of the systems. As reported in [30], in some cases, the minimum damping value has to be set up to 7% for achieving better performance of the systems Furthermore, here, the number of iterations, number of population, loudness, pulse emission rate, frequency minimum (f_{min}) and maximum (f_{max}) of BA are assumed to be 50, 50, 0.5, 0.6, 0, and 100, respectively.

5 Results and discussions

Several case studies are presented here in an attempt to investigate the performance of resilient wide-area MMC on the oscillatory stability of power system considering RPG and BESS. The 500 kV Java Grid in Indonesia is used as the test system. All the data as well as the power flow are taken from the Java-Indonesian electric grid. The generators are modelled into a ninth-order model, considering an exciter and governor. A modification has been made to the original system by integrating 300 MW aggregated WPP and 300 MW aggregated PV plant in Area 1 as well as 100 MW BESS in Area 2 as shown in Fig. 6. The PV plant is modelled into a sixth-order model, while the WPP is modelled into the eleventh-order model. Furthermore, BESS is modelled into the fifth-order model. Hence, the modified system consists of seven synchronous generators, one aggregated model of PV plant, WPP, and BESS (the original Java system only consider the conventional generator). Furthermore, there are 85 state variables in the modified system (the state variables of the original Java system are 72).

The WPP and PV plants are assumed to be operated at the maximum power point. As reported in [31], the Java system has two critical modes, inter-area and local mode 2. The generator that contributes to this critical modes are generators at bus 3 and bus 5 (hereafter denoted as *G*3 and *G*5). Table 1 shows the electromechanical (EM) mode damping and generators that contribute to the particular mode of Java system with RPG and BESS.

Here, four different scenarios are considered for comparative assessments. Table 2 illustrates the scenarios that used here. The PSO technique is used to design POD for Scenario 1. Grey wolf

Table 2 Different scenarios for simulation study

Number	Scenario
1	with traditional POD
2	with resilient wide-area POD in BESS
3	with resilient wide-area MMC in G_3, G_5, and BESS
4	with resilient wide-area MMC based on BA algorithm in G_3, G_5, and BESS (i.e. proposed method)

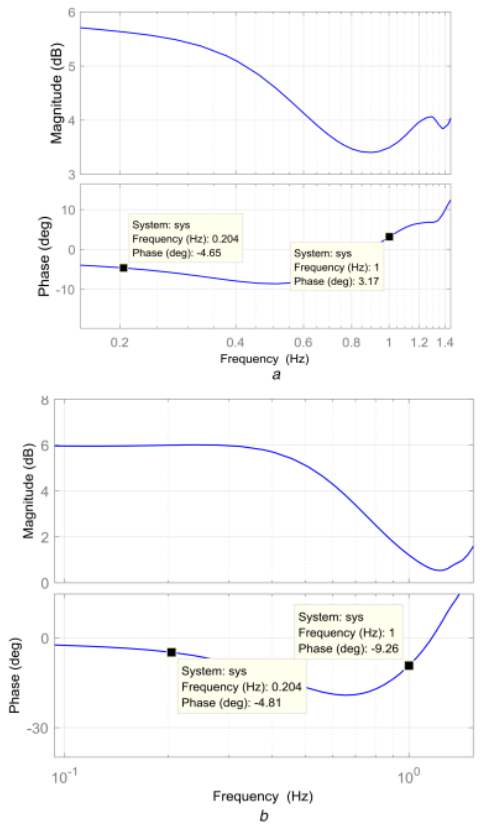

Fig. 7 *Bode plot of Vt/Vr transfer function*
(a) Generator 3, ***(b)*** Generator 5

Table 3 Damping ratio comparison for resiliency analysis

Case	Local 2	Inter-area
normal condition	46.45	94.17
loss of signals	42.18	77.26
BESS controller failure	40.23	67.52
*G*3 controller failure	40.53	52.44
*G*5 controller failure	27.01	35.44
*G*3 and *G*5 controller failure	7.94	24.94

optimiser is used to design the resilient wide-area POD at BESS in Scenario. For Scenario 3, the modified DE algorithm is used. For the last scenario (i.e. scenario 4), the BA algorithm is used. It should be noted that for scenarios 1 and 2, the simple Padé approximation time delay is used, while in the scenarios 3 and 4, two-stage time delay is used. The controller parameters are given in the Appendix. To check whether the proposed controller has achieved the WECC standard regarding the oscillation damping in power system, bode diagram analysis is performed here.

Figs. 7*a* and *b* illustrate the bode diagram of voltage terminal divided by voltage reference (V_t/V_r) transfer function. The phase angle of G_3 and G_5 is $<\pm 30°$ for the frequency range of 0.2 to 1.0 Hz. Hence, it can be stated that the proposed controller could achieve the WECC standard for oscillation damping.

5.1 Resiliency assessment

To test the efficacy of the proposed control method against the communication failure and any other controller failure, the damping performance of the critical mode is investigated. The global signal is disabled to emulate the loss of control input signal. Furthermore, to simulate the damping controller failure, the signal input to the controller is disabled. It should be noted that the scenario 4 is used for this study.

Table 3 shows the damping performance of the system under different cases. It is found that the damping of local mode 2 and inter-area mode deteriorated under communication and control failures. When controller failure emerges in BESS, *G*3, and *G*5, the damping performance is smaller than the normal condition. The worst condition is incurred when control failure emerges at *G*3 and *G*5 locations simultaneously. However, even in the worst condition, the damping ratio is relatively high (higher than the threshold value, 5%). Hence, it can be stated that the proposed controller is robust enough against the communication signal and control failure.

5.2 Time delay variation

In this subsection, investigation of the time delay variation on the system dynamics is performed. The damping ratio is evaluated to analyse the impact of different time delays in the system dynamics. Global time delay for controller output is varied from 100 until 700 ms in 100 ms step. Furthermore, the local time delay of the BESS controller output is also varied from 100 to 150 ms in steps of 10 ms. It should be noted that only scenario 4 is used in this investigation. Figs. 8*a* and *b* shows the inter-area and local mode 2 damping for various time delays.

It is noticeable that the time delay variation has significant influence on the system dynamic performance as indicated by the movement of the damping value in Figs. 8*a* and *b*. It is observed that the damping performance of inter-area mode is increased when the time delay is increased. In contrast, the damping performance of local mode 2 is deteriorated when time delay is increased. However, even with time delay variations, the damping performance of both mode is still high (above CIGRE standard) and the system is robust. Furthermore, it is evident that the correlation between time delay and damping is complex. The similar conclusion is also reported in [32].

5.3 Variation of operating condition

To assess the performance of the proposed controller, ten different operating conditions are used. Table 4 illustrates the operating conditions used for controller performance assessment.

The damping ratio of the local mode 2 and inter-area mode are depicted in Table 5. It should be noted that the BC is referred to the modified system for which the proposed controller is designed. It is found that the damping performance of the local mode is above the minimum (5%) standard under different operating conditions. Similar trends are observed for inter-area mode. Hence, it can be stated that the system with proposed controller is robust enough against different operating conditions.

5.4 System performance assessment and ranking

In this section, the system performance is assessed by using the control method criterion (given in the Appendix). To assess IAE, ISE, and ITAE, the rotor speed of the generator that contribute to the critical mode is used. The minimum the values of IAE, ISE, and ITAE indicate the better performance of the system. Table 6 shows the system performance assessment comparison on different scenarios. It is found that among all the performance assessment criterion, the scenario 4 (proposed controller) provides the best results.

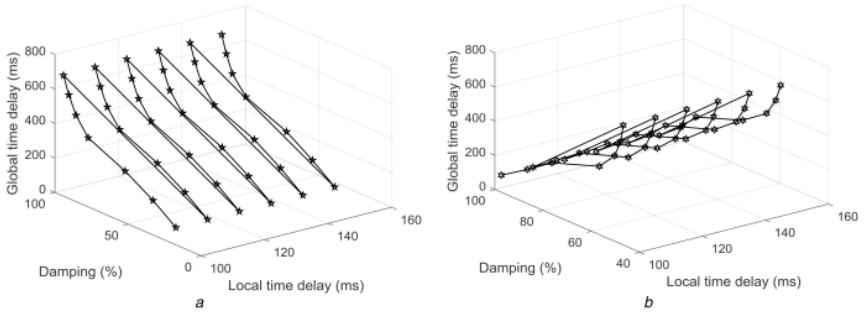

Fig. 8 *Damping ratio for time-delay variations*
(a) Inter-area mode, ***(b)*** Local mode 2

Table 4 Operating conditions for Java system

Operating condition	Changed system topologies from base case
OC1	G_2 output is 991.35 MW and load demand in bus 9 and 10 are 217.125 MW and 410.625 MW
OC2	G_3 output is 711 MW and load demand in bus 17 and 21 are 329.625 MW and 149.625 MW
OC3	G_5 output is 675 MW and load demand in bus 19 is 635 MW
OC4	G_6 output is 675 MW and load demand in bus 19, 23 and 24 are 539 MW, 529.125 MW and 777.75 MW
OC5	G_1 output is 1605.8 MW and load demand in bus 18 and 25 are 499 MW and 396 MW
OC6	G_2 output is 1540 MW and load demand in bus 14 and 12 are 1249 MW and 733.7 MW
OC7	Load demand in bus 15, 16, 17 and 21 are 1296 MW, 536.6 MW, 329.6 MW and 149.6 MW
OC8	Load demand in bus 11, 13, 20 and 22 are 915 MW, 810 MW, 384 MW and 227.3 MW
OC9	Load demand in bus 11, 12, 13, 14, 15, 16, 17, 18, 20, 21, 22 and 25 are 865, 683, 760, 1099, 1146, 486, 279, 449 , 334, 149.5, 227, and 396 MW
OC10	G_1, G_2 and G_3 output are 1605.8, 1540, and 711 MW

Table 5 Damping ratio at different operating conditions

Operating condition	Local 2	Inter area
BC	46.45	94.17
OC1	33.50	77.78
OC2	38.57	72.37
OC3	37.10	81.04
OC4	37.12	80.66
OC5	40.86	74.98
OC6	40.99	75.33
OC7	40.56	77.73
OC8	40.74	75.37
OC9	40.89	74.98
OC10	42.89	78.07

Q7 [a]BC = Base case.

Table 6 System performance assessment

Index	Scenario 1	Scenario 2	Scenario 3	Scenario 4
IAE	3.314×10^{-5}	4.88×10^{-5}	1.33×10^{-5}	5.96×10^{-6}
ISE	2.04×10^{-10}	2.87×10^{-10}	6.72×10^{-11}	1.21×10^{-11}
ITAE	1.53×10^{-4}	2.9×10^{-4}	4.24×10^{-5}	2.32×10^{-5}

To rank the controller performance the method given in Section 3 is used. Fig. 9 illustrates the controller performance and ranking for various scenarios. It is found that the proposed control method (scenario 4) is superior in performance enhancement and the robustness.

5.5 Comparative assessment

The damping ratio of the EM mode is used to investigate the performance of the proposed controller compared to other controllers. Table 7 illustrates the comparison of the damping ratio of the critical modes in all four scenarios. It is observed that the best damping performance is achieved by Scenario 4.

To validate the damping performance analysis, time domain simulations are also performed. A large perturbation is made in the system by a line outage between bus 17 and bus 9 to observe the oscillatory condition of the system. All of the scenarios are performed in the same operating and loading condition. The rotor speed of *G*3 and *G*5 are plotted as they contributed to the inter-area mode and local mode 2. Fig. 10*a* illustrates the rotor speed responses of *G*3, while Fig. 10*b* shows the G5 rotor speed responses. It is found that the best response is provided by scenario

4 (proposed controller) as indicated by the smallest overshoot and fastest settling time.

5.6 Comparison with other meta-heuristic methods

In this section, different meta-heuristic methods are compared for resilient wide-area-based MMC design. The comparison among the PSO, differential evolution algorithm (DEA), grey wolf optimiser (GWO), and BA (BA) has been made here. The objective functions for these three algorithms are the same as in (13). Fig. 11 shows the rotor speed responses of $G3$ under different heuristic approaches. From Fig. 11, it is found that in terms of time domain simulation, PSO, DEA, GWO, and BA give similar results. However, by using BA, it is found that the response is slightly improved in terms of overshoot. BA provides less overshoot than PSO, DEA, and GWO.

Fig. 12 illustrates the execution time of PSO, DEA, and BA for resilient wide-area MMC design using (13) as the objective function. It is found that BA provides fastest execution time compared to PSO, DEA, and GWO. This execution time is expected to increase with the size and complexity of in the system. Hence, by using BA, the execution time can be reduced.

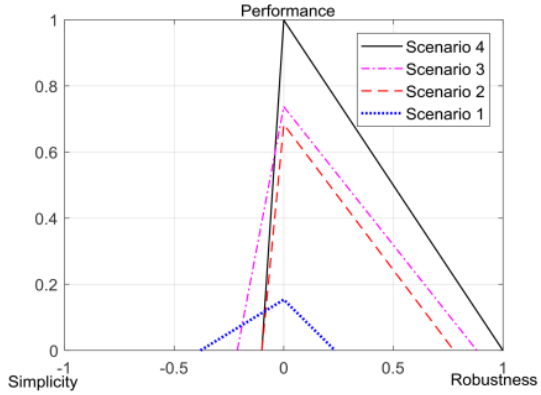

Fig. 9 *Controller ranking*

6 Conclusions

To deal with the communication and control failures in a wide-area control for oscillation damping, this paper proposed a BA-based resilient wide-area MMC for BESS and synchronous generators. Detailed simulation studies are conducted in a representative dynamic model of Java 500 kV transmission system. The communication and controller failures are both tested here. Based on the numerical analysis it is apparent that the proposed resilient wide-area MMC can maintain the satisfactory damping under communication channel or controller failure. Moreover, the proposed controller has advantages over other POD controllers in terms of IAE, ISE, and ITAE. In a word, the BA-based resilient wide-area MMC can achieve a satisfactory damping performance even though the operating conditions vary significantly or severe communication and control failures occurred in the system. Moreover, the execution time for BA-based wide-area control design is lower than the other meta-heuristic algorithms. Finally, the significant novelties of this paper with other works can be summarised as:

a. Both the communication and controller failure are considered in this work.
b. The local and global time delays are used for the analysis. Moreover, the time delays to and from the controller are also used for the controller design.
c. The BA with multi-objective function is used for the controller design.
d. The utilisation of multi-mode POD controller integrated into the exciter of the generator and BESS has been demonstrated.

7 Acknowledgments

The first author would like to thank the Ministry of Finance of Indonesian Government for awarding the Endowment Fund of

Table 7 Damping performance at different scenarios

Mode index	Scenario 1	Scenario 2	Scenario 3	Scenario 4
inter-area	5.72	15.59	20.30	94.17
local 1	10.12	8.75	9.29	8.45
local 2	4.13	7.70	15.50	46.45
local 3	6.79	6.27	6.63	6.39
local 4	7.36	6.26	6.37	7.08
local 5	22.68	26.84	26.84	26.84
local 6	22.84	18.09	18.09	18.09

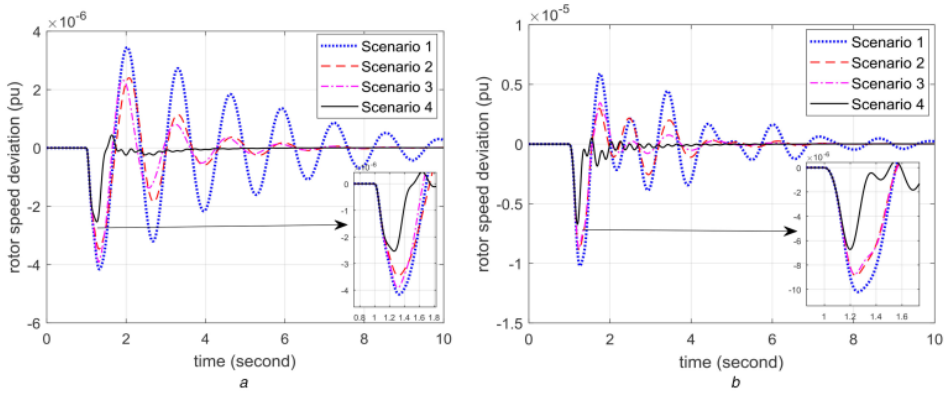

Fig. 10 *Rotor speed responses*
(a) Generator 3, ***(b)*** Generator 5

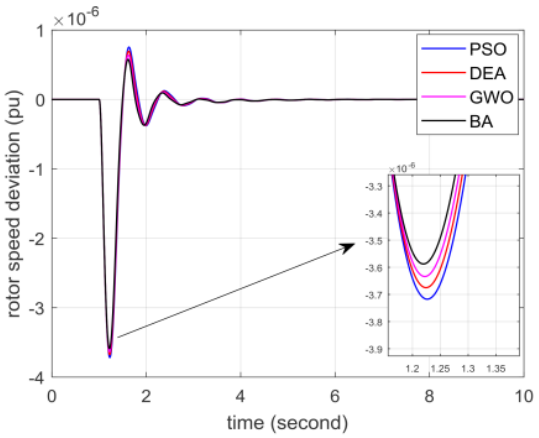

Fig. 11 *Rotor speed of G3 under different heuristic approaches*

1
Education Scholarship (LPDP) to pursue Ph.D. research at the University of Queensland, Australia.

8 References

[1] Hannan, M.A., *et al.*: 'Artificial intelligent based damping controller optimization for the multi-machine power system: a review', *IEEE. Access.*, 2018, **6**, pp. 39574–39594

Q2 [2] Pan, Y., *et al.*: 'Towards the robust small-signal stability region of power systems under perturbations such as uncertain and volatile wind generation', *IEEE Trans. Power Systems*, 2018, **33**, (2), pp. 1790–1799

[3] Setiadi, H., Krismanto, A.U., Mithulananthan, N., *et al.*: 'Modal interaction of power systems with high penetration of renewable energy and BES systems', *Int. J. Electr. Power Energy Syst.*, 2018, **97**, pp. 385–395

[4] Yorino, N., Abdillah, M., Sasaki, Y., *et al.*: 'Robust power system security assessment under uncertainties using bi-level optimization', *IEEE Trans. Power Systems*, 2018, **33**, (1), pp. 352–362

[5] Huang, H., Chung, C., Chan, K.W., *et al.*: 'Quasi-Monte carlo based probabilistic small signal stability analysis for power systems with plug-in electric vehicle and wind power integration', *IEEE Trans. Power Systems*, 2013, **28**, (3), pp. 3335–3343

[6] Guo, C., Liu, W., Zhao, J., *et al.*: 'Impact of control system on small-signal stability of hybrid multi-infeed HVDC system', *IET Gener. Transm. Distrib.*, 2018, **12**, (19), pp. 4233–4239

[7] El-Shimy, M., Sharaf, A., Khairy, H., *et al.*: 'Reduced-order modelling of solar-PV generators for small-signal stability assessment of power systems and estimation of maximum penetration levels', *IET Gener. Transm. Distrib.*, 2018, **12**, (8), pp. 1838–1847

[8] Ma, J., Qiu, Y., Li, Y., *et al.*: 'Research on the impact of DFIG virtual inertia control on power system small-signal stability considering the phase-locked loop', *IEEE Trans. Power Systems*, 2017, **32**, (3), pp. 2094–2105

[9] Bian, X.Y., Geng, Y., Lo, K.L., *et al.*: 'Coordination of PSSs and SVC damping controller to improve probabilistic small-signal stability of power system with wind farm integration', *IEEE Trans. Power Systems*, 2016, **31**, (3), pp. 2371–2382

[10] Zhou, Y., Li, Y., Liu, W., *et al.*: 'The stochastic response surface method for small-signal stability study of power system with probabilistic uncertainties in correlated photovoltaic and loads', *IEEE Trans. Power Systems*, 2017, **32**, (6), pp. 4551–4559

[11] Deeba, S.R., Sharma, R., Saha, T.K., *et al.*: 'Evaluation of technical and financial benefits of battery-based energy storage systems in distribution networks', *IET Renew. Power Gener.*, 2016, **10**, (8), pp. 1149–1160

[12] Akram, U., Khalid, M.: 'A coordinated frequency regulation framework based on hybrid battery-ultracapacitor energy storage technologies', *IEEE. Access.*, 2018, **6**, pp. 7310–7320

[13] Chandra, S., Gayme, D.F., Chakrabortty, A.: 'Coordinating wind farms and battery management systems for inter-area oscillation damping: a frequency-domain approach', *IEEE Trans. Power Systems*, 2014, **29**, (3), pp. 1454–1462

[14] Lu, C., Wu, X., Wu, J., *et al.*: 'Implementations and experiences of wide-area HVDC damping control in China southern power grid'. IEEE Power and Energy Society General Meeting, 2012

Q3 [15] Ray, S., Venayagamoorthy, G.K.: 'Real-time implementation of a measurement-based adaptive wide-area control system considering communication delays', *IET Gener. Transm. Distrib.*, 2008, **2**, (1), pp. 62–70

[16] Surinkaew, T., Ngamroo, I.: 'Two-level coordinated controllers for robust inter-area oscillation damping considering impact of local latency', *IET Gener. Transm. Distrib.*, 2017, **11**, (18), pp. 4520–4530

[17] Shen, Y., Yao, W., Wen, J., *et al.*: 'Resilient wide-area damping control using GrHDP to tolerate communication failures'. *IEEE Trans. Smart Grid*, 2018, pp. 1–1

Q4 [18] Chitara, D., Niazi, K.R., Swarnkar, A., *et al.*: 'Cuckoo search optimization algorithm for designing a multimachine power system stabilizer', *IEEE Trans. Industry Applications*, 2018, **54**, (4), pp. 3056–3065

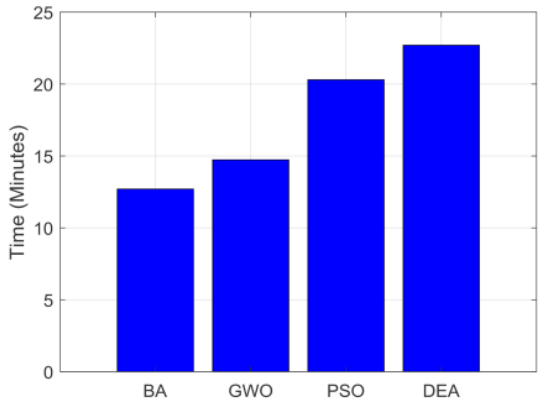

Fig. 12 *Comparison of execution time*

[19] Wang, S.-K.: 'Coordinated parameter design Of power system stabilizers And static synchronous compensator using gradual hybrid differential evaluation', *Int. J. Electr. Power Energy Syst.*, 2016, **81**, pp. 165–174

[20] Li, P., Xu, D., Zhou, Z., *et al.*: 'Stochastic optimal operation of microgrid based on chaotic binary particle swarm optimization', *IEEE Trans. Smart Grid*, 2016, **7**, (1), pp. 66–73

[21] Bai, W., Eke, I., Kwang Lee, Y.: 'An improved artificial bee colony optimization algorithm based on orthogonal learning for optimal power flow problem', *Control Eng. Pract.*, 2017, **61**, pp. 163–172

[22] Zhou, J., *et al.*: 'A multi-objective multi-population ant colony optimization for economic emission dispatch considering power system security', *Appl. Math. Model.*, 2017, **45**, pp. 684–704

[23] Lu, C.-F., Liu, C.-C., Wu, C.-J.: 'Dynamic modelling of battery energy storage system and application to power system stability', *IEE Proc., Gener. Transm. Distrib.*, 1995, **142**, (4), pp. 429–435

[24] 'WECC guide for representation of photovoltaic systems in large-scale load flow simulation'. WECC Renewable Energy Modeling Task Force Report, 2010

[25] 'Standard report for Variable generation'. NERC Special Report, Atlanta, GA, 2010

[26] Clark, K., Miller, N.W., Walling, R.: '*Modelling of GE solar photovoltaic plants for grid studies*' (General Electrical International, Inc., Schenectady, NY, 2010)

[27] Zou, Y., He, J.: 'Comprehensive modeling, simulation and experimental validation of permanent magnet synchronous generator wind power system'. IEEE/IAS 52nd Industrial and Commercial Power Systems Technical Conf. (I&CPS), 2016

[28] Zhang, Y., Preece, R.: 'A comprehensive methodology for assessing power oscillation damping controllers for HVDC-based system stabilization'. IEEE Eindhoven PowerTech, 2015

[29] Yang, X.-S.: 'A New metaheuristic Bat-inspired algorithm'. Nature Inspired Cooperative Strategies for Optimization (NICSO 2010): Springer, Berlin, 2010

[30] Pal, B., Chaudhuri, B.: '*Robust control in power systems*' (Springer Science & Business Media, 2006)

Q5 [31] Setiadi, H., Mithulananthan, N., Krismanto, A.U., *et al.*: 'Low-frequency oscillatory stability study on 500 kV java-Indonesian electric grid'. IEEE 27th Int. Symp. on Industrial Electronics (ISIE), 2018

[32] Jia, H., Cao, X., Yu, X., *et al.*: 'A simple approach to determine power system delay margin'. IEEE Power Engineering Society General Meeting, 2007

[33] Paserba, J.: 'Analysis and control of power system oscillation', *CIGRE Technical Brochures*, 1996, **38**, (7)

Q6 [34] WECC-0107 Power System Stabilizer (PSS) Design and Performance WECC Regional Reliability Standard, VAR-501-WECC-3-Power System Stabilizer, 2016

[35] Marlin, T.E.: '*Process control, designing processes and control systems for dynamic Performance*' (McGraw-Hill, New York, 1995)

[36] Padhy, B.P., Srivastava, S.C., Verma, N.K.: 'A wide-area damping controller considering network input and output delays and packet drop', *IEEE Trans. Power Systems*, 2017, **32**, (1), pp. 166–176

[37] Shakarami, M., Davoudkhani, I.F.: 'Wide-area power system stabilizer design based on grey wolf optimization algorithm considering the time delay', *Electr. Power Syst. Res.*, 2016, **133**, pp. 149–159

9 Appendix

9.1 Industry standard related to oscillation damping

The damping ratio of the mode is used to investigate how fast the oscillation can be damped. Based on the International Council on Large Electric Systems (CIGRE), the minimum damping ratio allowed the power systems is in the range of 3–5% [33]. However,

Table 8 Control parameters

Scenario	Controller value
1	K_{pod} = 250 pu, Tw = 0.1215 s, T_1 = 0.00893 s, T2 = 0.0203 s
2	$K_1 = K_2$ = 70 pu, $K\Delta\omega$ = 5, $K\Delta pe$ = 1.462, T_1 = 0.05 s, T_2 = 0.02 s, T_3 = 0.03 s, T_4 = 0.01 s, $Tw2$ = 10 s, $Tw3$ = 10 s
3	$K_1 = K_2$ = 40 pu, $K\Delta\omega$ = 10.97, $K\Delta pe$ = 1.567, T_1 = 0.06 s, T_2 = 0.05 s, T_3 = 0.06 s, T_4 = 0.08 s, $Tw2$ = 15.955 s, $Tw3$ = 13.667 s
4	K_1 = 90.95 pu, K_1 = 90.07 pu, $K\Delta\omega$ = 19.999, $K\Delta$pe = 1.991, T_1 = 0.0754 s, T_2 = 0.0987 s, T_3 = 0.0998 s, T_4 = 0.1 s, Tw2 = 19.996 s, $Tw3$ = 19.942 s

without the loss of generality we choose the highest value, 5%, here. Hence, any mode with damping ratio lower than 5% is classified here as the critical mode. Therefore, it is important to design the oscillation damping that could achieve this standard. Furthermore, synthesising the oscillation damping control itself has another standard that need to be fulfilled.

The WECC has reported a standard regarding the oscillation damping in power systems. It has been stated that the oscillation damping shall be set to provide the measured, simulated or calculated compensated transfer function of voltage terminal divided by voltage reference (V_f/V_r) in the frequency domain of the excitation system such that the phase angle should not exceed ± 30° for the frequency range from 0.2 to 1 Hz [34].

9.2 Measuring the control systems performance

Indices are used to measure the control system performance against disturbances. Integral of absolute error (IAE) and integral of squared error (ISE) are the typical indices for assessing the system performance. Furthermore, more comprehensive indices as a function of time are developed. Integral time absolute error (ITAE) is the performance indices that consider time in the calculation. Here, IAE, ISE, and ITAE are used to assess the system performance. The mathematical representation of IAE, ISE and ITAE can be described as [35]:

$$\mathrm{IAE} = \int_0^{\mathrm{time}} |e(t)|\, dt \tag{15}$$

$$\mathrm{ISE} = \int_0^{\mathrm{time}} (e(t))^2\, dt \tag{16}$$

$$ITAE = \int_0^{\mathrm{time}} t|e(t)|\, dt \tag{17}$$

9.3 Time delay model

To capture the time delay for the dynamic simulation a two-step time delay model is used. A two-step time delay can be modelled for the signal delay coming from the input and the output of the network [36]. To capture the communication delay of the network, Padé approximation approach is used. The transfer function to represent the Padé approximation time delay can be described as [37]:

$$e^{-s\mathrm{Td}} = \frac{1 - K_1 s + K_2 s^2 + \cdots \pm K_n s^n}{1 + K_1 s + K_2 s^2 + \cdots \pm K_n s^n} \tag{18}$$

In (18), K_1, K_2, …, K_n are the constant coefficients and n is the order of approximation. As reported in [37], the dynamic behaviours of the first-order and the second-order time delays are similar. Hence, the first-order Padé approximation is considered to be sufficient to represent the latency in power systems.

9.4 Controller value

Table 8 illustrates the controller value used here.

Author Queries

Q	Please make sure the supplied images are correct for both online (colour) and print (black and white). If changes are required please supply corrected source files along with any other corrections needed for the paper.
Q1	Please reduce the number of words in the Abstract to 200 words.
Q2	As per the journal style, names of only first three authors are to be provided. If there are more than three, only the first three should be given followed by et al. Please provide the missing author names in Refs. [1, 2, 22].
Q3	Please provide place of conference in Refs. [14, 27, 28, 31, 32].
Q4	Please provide volume number in Ref. [17].
Q5	Please provide the location of the publisher (country) in Ref. [30].
Q6	Please provide page range in Ref. [33].
Q7	Please provide link for this note in Table 5

Resilient wide-area multi-mode controller design based on Bat algorithm for power systems with renewable power generation and battery energy storage systems

ORIGINALITY REPORT

5%	0%	0%	5%
SIMILARITY INDEX	INTERNET SOURCES	PUBLICATIONS	STUDENT PAPERS

PRIMARY SOURCES

1	Submitted to Central Queensland University Student Paper	5%

Exclude quotes	On	Exclude matches	< 2%
Exclude bibliography	On		